Specific oligodendrocyte populations have differential spatial distribution and susceptibility to injury

Elisa M. Floriddia[1*], Shupei Zhang[1], David van Bruggen[1], João P. Gonçalves dos Santos[1], Müge Altınkök[1], Sarah Förster[2], Richa B. Tripathi[3], William D. Richardson[3], Robin J.M. Franklin[2], Gonçalo Castelo-Branco[1,4*]

[1] Laboratory of Molecular Neurobiology, Department Medical Biochemistry and Biophysics, Karolinska Institutet, Biomedicum, 17177 Stockholm, Sweden

[2] Wellcome Trust-Medical Research Council Cambridge Stem Cell Institute, Clifford Allbutt Building, Cambridge Biomedical Campus, University of Cambridge, Cambridge CB2 0AH, UK.

[3] Wolfson Institute for Biomedical Research, University College London (UCL), Gower Street, London WC1E 6BT, UK.

[4] Ming Wai Lau Centre for Reparative Medicine, Stockholm node, Karolinska Institutet, 171 77 Stockholm, Sweden

[*]Co-correspondence: goncalo.castelo-branco@ki.se

elisa.floriddia@ki.se

One Sentence Summary: Different location and response to injury by mature oligodendrocytes

Abstract

Oligodendrocytes (OLs), the myelinating cells of the central nervous system, are transcriptionally heterogeneous, the origin and functional consequences of which are unknown. We report that mature OL2 (MOL2) preferentially distribute in the spinal cord white matter, while MOL5/6 are abundant in the brain and in the spinal cord grey matter. Remarkably, MOL2 and MOL5/6 segregate around sensory and motor tracts in the spinal cord, respectively. Lineage tracing, single-cell RNA-Sequencing and RNAscope ISH indicated that the developmental origin does not specify OL progenitors into MOL populations. Following spinal cord injury, we observed depletion of MOL2, while MOL5/6 abundantly repopulate the injury site. Thus, specific MOL populations, identified by scRNAseq, have spatial preference and differential responses to disease, suggesting that OLs are both transcriptionally and functionally heterogeneous.

Main text

OLs insulate and metabolically support axons, increasing conduction speed (*1*). We have recently reported that the OL lineage is formed of transcriptionally distinct subpopulations/states during development and disease (*2-4*). Heterogeneity of the OL lineage might not lie exclusively on the OL cell transcriptome. Indeed, developmentally distinct Oligodendrocyte Progenitor Cell (OPC) pools generate OL lineage cells with differential abilities to respond to demyelination (*5*), OLs form myelin internodes of various length and thickness, also along the same axon (*6, 7*), properties regulated at both cell-autonomous and non-autonomous level (*8, 9*). Additionally, remyelination occurs at faster rate in white compared to grey matter (*10*). Nevertheless, it is unclear whether the transcriptional heterogeneity of the OL lineage is associated with functional heterogeneity.

The potential functional heterogeneity of mature OLs (MOLs) is likely to correlate with their local environment and neuronal network. While single-cell RNA-sequencing (scRNAseq) suggests differential enrichment of MOLs in different regions of the CNS (*2*), technical limitations, such as differential viability of cell subpopulations to tissue dissociation (*11, 12*), might lead to biased enrichment. Thus, we assessed the distribution of the OL lineage within brain and spinal cord white matter (WM) and grey matter (GM. Fig. 1A-B). We performed IHC and RNAscope ISH for Sox10 as a pan marker of the OL lineage and analyzed high-resolution tiled *z*-stack confocal images of the corpus callosum (WM), somatosensory cortex (GM) and spinal cord dorsal horn (GM) and white matter with a custom automated image analysis pipeline (CellProfiler, validation in Fig. S1A-B and Methods). To analyze the spatial distribution of oligodendrocyte subpopulations/states, we selected specific markers based on their unique or substantially higher expression based on scRNAseq data (*2, 3*). *Ptprz1* (receptor-type tyrosine-protein phosphatase zeta 1), a marker of OPCs and committed

OPCs (COPs), presented a homogeneous distribution across the analyzed regions (Fig. 1C, G; Fig. S2A, E). We observed a marked decrease from the juvenile to adult CNS stages, in particular in the somatosensory cortex (from 36.91 ± 2.98% at P20 to 11.73 ± 2.23% at P60, Fig. 1C, G; Fig. S2A, E). The loss of OPCs and COPs correlates with reduced ability of the mouse CNS to regenerate after demyelination (*5, 13-15*) and parallels their age-associated decrease in humans (*16*).

We previously described several transcriptionally distinct mature oligodendrocyte populations (*2-4*). Since MOL1, MOL2, and MOL5/6 present the most distinct gene marker modules (*2-4*), we focused on these populations to investigate their spatial distribution. *Egr2* (Early Growth Response 2; also known as *Krox20*) is expressed specifically by MOL1 in the OL lineage (*2*), even though at low levels (average molecule count of one in scRNAseq (*2*). With RNAscope ISH, we observed a count of 10 ± 1.86 mRNA molecules and a homogeneous distribution of MOL1 within the analyzed regions (Fig. 1F, J; Fig. S2D, H). There was a consistent trend towards decreasing numbers of MOL1 with age, although statistically non-significant (27.83 ± 5.93% in the somatosensory cortex, 25.71 ± 5.0.5% in the corpus callosum, and 25.26 ± 8.14% in the dorsal horn at P20 and 16.46 ± 7.87%, 15.44 ± 5.97%, and 11.89 ± 4.51% at P60, respectively; Fig. 1F, J; Fig. S2D, H).

Klk6 (Kallikrein Related Peptidase 6) is a marker for MOL2 (*2-4*). The average molecule count of *Klk6* in MOL2 is 27 per cell in the scRNAseq (*2*). Accordingly, *Klk6* signal in RNAscope ISH was robust and generated clusters of fluorescent signal that could not be reliably segmented for single molecule quantification, but allowing cellular quantification. We observed a very low number of *Klk6*$^{+}$ OLs in brain regions such as the somatosensory cortex (3.49 ± 0.96% at P20 and 3.24 ± 0.97% at P60) and corpus callosum (0.23 ± 0.12% at P20 and 0.39 ± 0.18% at P60. Fig. 1E, I, Fig. S2C, G). Strikingly, MOL2 constitute 15.34 ± 2.36% and 16.27 ± 1.37% of the OL lineage in the GM and WM of the spinal cord of the P20 and P60 spinal cord, respectively (Fig. 1E, I, Fig. S2C, G). As such, MOL2 is a population specifically enriched in the spinal cord.

MOL5/6 express *Ptgds* (Prostaglandin D2 Synthase. (*2-4*), which showed an average molecule count of 117 in scRNAseq (*2*). At P20, MOL5/6 were more abundant in the spinal cord GM (24.71 ± 3.08%) compared to the somatosensory cortex (10.24 ± 1.84%) and corpus callosum (9.39 ± 2.08%) (Fig. 1D, H, SFig. 2B, F). During adulthood, MOL5/6 increased significantly in all regions, being slightly more abundant in WM corpus callosum (63.77 ± 6.31%) compared to GM somatosensory cortex (54.43 ± 3.51%) and GM dorsal spinal cord (51.37 ± 3.14%. Fig. 1D, H, SFig. 2B, F).

Interestingly, MOL2 and MOL5/6 are differentially distributed in the spinal cord. We observed a preferential localization of MOL2 in the white matter compared to the grey matter of the spinal cord (Fig. 2B, C), which is maintained with age (25.13 ± 2.31% at P20 and 24.83 ± 1.92% at P60 in the WM). In contrast, the MOL2 population decreases in the grey matter of the spinal cord during adulthood (15.26 ± 1.87 at P20 and 7.16 ± 1.15% at P60. Fig. 2C). When we analyzed the distribution of MOL5/6, we observed that MOL5/6 preferentially distribute instead in the grey matter (30.07 ± 3.19% and 51.37 ± 3.14%) compared to the white matter of the spinal cord (14.31 ± 2.04% and 11.97 ± 2.78% at P20 and P60. Fig. 2F, G).

We further assessed whether there was spatial preference where functionally distinct axonal tracts run in the spinal cord (Fig. 2A). We analyzed the descending motor dorsal corticospinal tract, where we observed an increased number of OLs with age (55.73 ± 5.29% and 70.91 ± 1.9% of total nuclei at P20 and P60, respectively. Fig. S1C), and the ascending dorsal column tract, where there was no significant difference in the OL lineage distribution with age (62.65 ± 4.5% and 66.64 ± 1.8% of total nuclei at the dorsal column at P20 and P60, respectively. Fig. S1C). The majority of MOL2 are found at the level of the ascending sensory dorsal column tract (19.32 ± 3.18% and 24.26 ± 1.83% within the dorsal column and 5.33 ± 1.35% and 5.25 ± 0.8% within the dorsal corticospinal tract at P20 and P60, respectively. Fig. 2D, E). Also in this instance, we observed that MOL2 and MOL5/6 present complementary distributions. MOL5/6 have a higher density and preferentially localize in the dorsal corticospinal tract (19.69 ± 6.67% and 50.91 ± 8.37% at P20 and P60, respectively) compared to the dorsal column (12.88 ± 4.82% and 18.78 ± 1.97% at P20 and P60, respectively. Fig. 2H, I). Altogether, our data suggest that MOL2 have a preference for WM versus GM, and might have a preference for the sensory axons ascending to the brain compared to the motor axons descending along the spinal cord, while MOL5/6 populate areas where MOL2 are not prevalent.

The OL lineage derives from distinct embryonic lineages, which could play a role in the final distribution of MOL2 and MOL5/6 in the adult CNS. We evaluated the role of the domain of origin in OPC specification towards OL lineage subpopulations, by performing scRNAseq in OLs isolated from the Emx1::Cre-Sox10::GFP-TdTom mice (*2, 3, 17*). These mice allow us to discriminate between ventrally- and dorsally-derived OL lineage cells, which will express the eGFP and TdTom reporters, respectively (*17*). We focused on P60 corpus callosum (Fig. 3A), where OLs derived from the cortical plate (dorsal domain) as well as the lateral and medial ganglionic eminences (ventral domains of the embryonic forebrain) are represented (*17*). A greater proportion of $TdTom^+$ OL lineage was obtained, as expected (Fig. 3A, D. Fig. S3B. Table 1) (*17*). Clustering analysis with GeneFocus (*3, 18*) of 2,853 OL lineage cells led to the identification of the previously identified OL

lineage subpopulations (Fig. S3B. *2, 19*), including MOL2 and MOL5/6 (highlighted in Fig. 3C-D;). Strikingly, the contribution of ventrally- and dorsally-derived OL lineage cells to each cluster is comparable (Fig. 3C-D. Fig. S3B).

Ventral-derived OL lineages arise earlier during development than dorsal lineages (*43-45*). As such, we further performed lineage tracing using the Pdgfrα::CreER^{T1}-loxP-GFP mouse model (*20*) to fate map the progeny of pre-OPCs appearing at E12.5 (*3*) or OPCs at P3-5 (Fig. 3E). We observed that the progeny of E12.5 pre-OPCs do not disappear later on in life in any of the analyzed regions (Fig. 3F-G, Fig. S4A-F, I, E, M). Importantly, there was no significant difference in the contribution of the two developmental waves to the MOL1, MOL2, and MOL5/6 populations (Fig. 3F-G, Fig. S4A-M). While most of the MOL2 in the dorsal horn spinal cord were derived from E12.5 pre-OPCs at P20, the contribution from postnatally fate mapped OPCs reached comparable levels to the embryonically derived MOL2 in adulthood (19.09 ± 4.95% and 23.35 ± 1.28% from the postnatally- and embryonically-derived MOL2, respectively. Fig. S4K, M-N). This suggests that postnatally derived OPCs start differentiating into MOL2 later than embryonically derived OPCs. Altogether, our scRNAseq and lineage tracing data suggest that the domain and time of origin does not influence the OPC specification towards distinct MOL populations/states, and that, despite the different migratory paths of OPCs, their differentiation stage might be determined by their final localization.

The spatial preference of MOL2 and MOL5/6 for specific regions in the spinal cord might be associated with functional differences. Therefore, we asked whether these MOL populations differentially respond to injury in this area. Traumatic injury of the spinal cord is a chronic pathological condition that leads to loss of locomotor and sensory functions, depending on the injury level and its severity, through Wallerian axonal degeneration and demyelination of damaged and spared axons (*21, 22*). We performed dorsal funiculi transection, an injury model of moderate severity, resulting in the complete transection of the dorsal columns, dorsal corticospinal tract and partial damage of the dorsal horns (Fig. 4A). We then assessed the spatial distribution of MOL2 and MOL5/6 three and five months post injury, both at and away from the site of trauma (Fig. 4B-C), when partial remyelination occurs (*21*). Strikingly, we observed specific ablation of MOL2 at the injury site three months post-injury (3 mpi, Fig. 4F and Fig. S5A), a loss that is maintained at 5 mpi (Fig. 4E-G). In contrast, MOL5/6 abundantly re-populated the injury site over time (Fig. 4D-G. Fig. S5A), reaching up to 60.1 ± 4.8% of the OL lineage (Fig. 4G). SCI results in chronic loss of mature OLs both at and distant to the injury site (SFig. 5D-E. (*22-27*). We assessed whether the spatial distribution of MOL2 and MOL5/6 rostral and caudal to the injury site was affected by a potentially

OL loss biased towards specific populations (Fig. 4D-G. SFig. 5A-C). At the dorsal funiculi, MOL2 showed an increase with time, both dorsal and caudal to the injury (15.8 ± 3.19% and 45.94 ± 5.33% of the OL lineage at 3 and 5 mpi, respectively. Fig. 4D-G and SFig. 5A-B). This might underline a greater need of MOL2 in re-wired neural circuits during the chronic phase following injury. At the latter time point post injury, the MOL2 cell density is greater than that found in the white matter of the intact adult spinal cord, (24.83 ± 1.92% Fig. 2C). This potentially could have a functional impact, for example on consolidation of remodeled neural circuits or inhibition of ectopic synapse formation (*8, 28-32*). The contribution of MOL5/6 in the dorsal funiculi rostral and caudal to the injury does not change following injury (18.8 ± 2.82% and 18.75 ± 2.9% at 3 and 5 mpi, respectively. Fig. 4D-G and SFig. 5A, C), similar or somewhat increased compared to their contribution in the white matter of the intact adult spinal cord (11.97 ± 2.78%, Fig. 2G). However, spinal cord injury does not affect the spatial preference of MOL2 and MOL5/6 away from the injury site (Fig. 4D, Fig. S5A, F-I). In summary, our data shows that specific OL lineage populations have differential susceptibility to trauma and differential ability to re-populate the injury site.

Here, we unveiled the spatial preference of specific mature OL populations, the ability of OPCs from different developmental origins to equally generate mature OL subtypes, and the OL population-specific susceptibility to injury. We show that the number of MOL5/6, as well as the total number of OLs, increases in the CST from juvenile to adulthood. The CST is fully formed at birth, but the activity-dependent refinement of its terminations (elimination and addition of new targets) and myelination take place long into postnatal development (*33, 34*). Thus, the observed increased number of MOL5/6 correlates with the myelination pattern of the CST (*35*). We also observed an increased number of MOL5/6 in the corpus callosum with age. Both the CST and corpus callosum maintain plasticity throughout life essential for acquisition and maintenance of new motor skills with OL turnover continuing throughout life, suggesting that myelin needs to be constantly remodeled (adaptive myelination) for those axonal tracts (*36-38*). Altogether, our data suggest that MOL5/6 are an OL population associated with experience-dependent plasticity.

In contrast, we show that MOL2 preferentially locate in the dorsal columns, suggesting that MOL2 are associated with more stable neural circuits. Indeed, proprioceptive and mechanoreceptive long projecting axons are myelinated early in development and reach complete myelination by juvenile (*35, 37*), correlating with the high and stable enrichment of MOL2 in this region. MOL2 preferentially localize where highly myelinated long projecting sensory axons run in the spinal cord (*39, 40*). This may suggest that they produce myelin favoring fast conduction. Additionally, MOL2 are transiently over-produced in the grey matter of the spinal cord, suggesting that MOL2 selection

and correct localization might be regulated by intrinsic mechanisms, such as programmed cell death (*41, 42*)

Furthermore, we did not observe any developmental specification of OPCs into specific OL subpopulations/states. This observation fits a model where the mechanisms regulating differentiation of the OL lineage into mature subtypes are not dependent on the domain of origin (*43-45*) unlike neurons (*46-48*).

Axonal degeneration and demyelination are important features of SCI and other neurological diseases (*49*). The differential response of MOL2 and MOL5/6 to spinal cord injury paves the way to a much deeper understanding of their role in the context of demyelination and adult regeneration. Indeed, MOL2 and MOL5/6 might have differential contribution to remyelination, axonal support, action potential conduction, and synapse formation inhibition; all of which will be important for regeneration. Notably, in the context of multiple sclerosis, we have recently shown a decrease of specific human OL populations (*50*). Altogether, the present and recent studies show that specific mature OL populations are differentially susceptible to disease (*50*). It will be relevant to investigate whether those lost populations are signature of demyelinating pathology or disease specific. As such, correlation analysis and further investigation of the functional properties of mature OL populations can be expected to unveil important cellular targets to prevent their elimination or promote remyelination in the context of injury or pathology.

Acknowledgements

We would like to thank Rashid Holtinkoski, Eneritz Agirre, Ana Mendanha Falcão, Alessandra Nanni, Johnny Söderlund, Ahmad Moshref, Tony Jimenez-Baristain, the Facility Management and Administration at Biomedicum (Karolinska Institutet, Stockholm) for laboratory management and support. Dr. Göran Månsson and Connla Edwards at the Biomedicum Imaging Core Facility (Karolinska Institutet, Stockholm), Dr. Jaromir Mikes at the Mass Cytometry National Facility (SciLife Lab, Stockholm); Drs. Karolina Wallenborg, Anna Juréus, Marcela Ferella at the Eukariotic Single Cell Genomics facility (SciLife Lab, Stockholm); Katarina Ericsson, Kristoffer Tenebro Berglund, Johanna Hornstrand at the Comparative Medicine Biomedicum facility (Karolinska Institutet, Stockholm) and their respective facility managements, the National Genomics Infrastructure and Uppmax for providing assistance in massive parallel sequencing and computational infrastructure. The bioinformatics computations were performed on resources provided by the Swedish National Infrastructure for Computing at UPPMAX, Uppsala University. Work in G.C.-B.'s research group was supported by Swedish Research Council (grant 2015-03558),

European Union (Horizon 2020 Research and Innovation Programme/ European Research Council Consolidator Grant EPIScOPE, grant agreement number 681893), Swedish Brain Foundation (FO2017-0075), Ming Wai Lau Centre for Reparative Medicine, Strategic Research Programme in Neuroscience (StratNeuro) and Karolinska Institutet.

Author Contributions: E.M.F. and G.C.-B. conceived the project, designed the study and interpreted results. E.M.F. and S.Z. performed experiments and analyzed data. J.P.G.S. and M.A. performed experiments. D.vB. analyzed data. R.B.T. and W.D.R. shared and S.F. bred the Emx1::Cre-Sox10::Cre-LoxP-GFP-STOP-TdTom mice. E.M.F., S.Z., D.vB., S.F., W.D.R., R.J.M.F., and G.C.-B. discussed the results of the study. E.M.F. and G.C.-B. wrote the manuscript with feedback from all co-authors.

Materials and Methods

Animals

All experimental procedures were performed following the guidelines and recommendation of local animal protection legislation and were approved by the local committee for ethical experiments on laboratory animals in Sweden (Stockholms Norra Djurförsöksetiska nämnd).

Mouse lines used in this study are Pdgfrα::CreER^{T1}-RCE::LoxP-GFP(*20, 51*), Sox10::CreER^{T2}-ROSA26::LoxP-GFP(*52, 53*), available at The Jackson Laboratory, and Emx1::Cre-Sox10::Cre-LoxP-GFP-STOP-TdTom (*17*). Mice were used with the Cre allele in hemizygous and the reporter gene allele in hemizygous or homozygous.

Animals were sacrificed at juvenile (P20-21) and adult stages (P60, P90), injuries were performed on adult mice (P60-P90) and sacrificed three or five months post-injury. Both sexes were included in all experiments. The following light/dark cycle was used: dawn 6:00-7:00, daylight 7:00-18:00, dusk 18:00-19:00, night 19:00-6:00. Mice were housed to a maximum number of 5 per cage in individually ventilated cages with access to food and water *ad libitum*.

Lineage tracing

To fate map the OPCs generated at E13.5 and present at P3-5, Pdgfrα::CreER^{T1}-RCE::LoxP-GFP mice were used(*20, 51*). Time-mated females were injected i.p. with 1 mg of tamoxifen (Sigma) at pregnancy day E12.5 or 2 mg once daily when pups were P3 to P5 (tamoxifen reaching the pups via the mother's milk). The lower dose of tamoxifen during pregnancy (equivalenet to 33 mg/kg of body weight) was used to restrict the labeling to the first appearing OPCs. Indeed at this low dose, tamoxifen is metabolized within 24-36 h after injections (therefore E13.5-E14.0)(*54-57*). The litters

were then sacrificed at juvenile (P20) or adulthood (P60) and brains and spinal cords collected for tissue analysis by RNAscope ISH coupled with IHC.

Spinal cord injury and post-operative care

Mice were kept under anesthesia with a 2% isoflurane/O_2 mixture at 1 litre/minute, after two-three minutes induction with 5% isoflurane/O_2 mixture at 1 litre/minute. Body temperature was maintained by keeping the mice on a heating pad (37-39°C) during the whole procedure.

The injury site was mid-thoracic (T10). The fur was shaved and the area disinfected with Clinical (DAX. twice) and 70% EtOH (once). The skin was incised, the superficial fat displaced, the prominent vessel (between T7 and T8) was identified and used as reference point. Then, the muscle tissue over T9-11 removed to expose the vertebrae. A T10 laminectomy was performed, the dura mater was removed, and the dorsal funiculi transection was performed with a microknife. Dorsal funiculi transection damages dorsal columns, dorsal corticospinal tract, and partially the dorsal horns.

After surgery, the mice were injected i.p. with Buprenorphine (Temgesic®) 0.01 mg/kg of body weight and s.c. with 0.5 ml of 0.9% saline solution. The mice were then placed in their home cages and monitored until fully recovered from anaesthesia. Mice underwent daily checks for general health status, weight loss, mobility, wounds, swelling, infections, or autophagy of the toes. When mice lost weight after surgery, their diet was supplemented with DietGel® Recovery (Clear H_2O). The mice used in this study did not show self-induced wounds or autophagy of the toes or wound infections.

Tissue preparation and sectioning

At the end of the experiments for the visualization in tissue of the OL lineage populations, the animals were deeply anesthetized with ketamine (120 mg/kg of body weight) and xylazine (14 mg/kg of body weight) and transcardially perfused with 0.1 M PBS followed by 4% PFA in PBS (pH 7.4 for both solutions). Brains and spinal cords were dissected and post-fixed in 4% PFA in PBS (pH 7.4) at 4°C overnight and cryoprotected in 30% sucrose for 48-36 hours.

Tissue was embedded in Tissue-Tek® O.C.T. compound (Sakura). Both brains and spinal cords were coronally cryosectioned (20 and 16 µm, respectively) in 1:10 series. Sections were stored at -80°C until further use.

Tissue dissociation and single-cell RNAseq

The corpus callosum of P60 Emx1::Cre-Sox10::Cre-LoxP-GFP-STOP-TdTom(*17*) was microdissected from two mice and the tissue dissociated into a single-cell suspension, as previously

described (*2*). Briefly, mice were transcardially perfused with ice-cold oxygenated artificial cerebrospinal fluid (22 mM NaCl, 0.63 mM KCl, 0.4 mM NaH_2PO_4 * $2H_2O$, 6.5 mM $NaHCO_3$, 25 mM Saccharose, 5 mM Glucose, 0.5 mM $CaCl_2$, 4 mM $MgSO_4$. pH 7.3) and the brains collected. The tissue was sectioned at the vibrotome in ice-cold artificial cerebrospinal fluid and the corpus callosum microdissected. Tissue dissociation was performed with the Adult Brain Dissociation Kit (Miltenyi Biotec) following manufacturer's instructions (red blood cells removal step was not included). After debris removal, the cells were resuspended in ice-cold 1% BSA in artificial cerebrospinal fluid, filtered with 30 µm filter (Sysmex Partec) and FACS sorted with the BD Influx System (USB. BD FACS™) to separate GFP^+ and $TdTom^+$ OL lineage cells.

The sorted cells were processed with the Chromium Single Cell A Chip kit v2 and library prep with the Chromium Single Cell 3´Library & Gel Beads kit v2 (10X Genomics) accordingly to manufacturer's instructions. A total of 3,000 cells for each sample was loaded on the Chromium Single Cell A Chip, although a lower number of cells was recovered in singlet and passed the quality control.

RNAscope in situ hybridization (ISH) and immunostaining (IHC)

RNAscope ISH was performed using the RNAscope® Multiplex Fluorescent Detection Reagents Kit v2 (ACD Biotechne) on PFA fixed juvenile, adult, and injured brains and spinal cords accordingly to manufacturer's instructions with some modifications. Briefly, after treatment with boiling 1X target retrieval, the sections were incubated with Protease IV for 20 min at RT, followed by washing and the indicated hybridization and amplification steps. Probes used in this study were designed for mouse *Sox10*-C1 or -C2 (ACD Biotechne, 435931), *Ptgds*-C1 (ACD Biotechne, 492781), *Klk6*-C3 (ACD Biotechne, 493751), *Egr2*-C3 (ACD Biotechne, 407871), *Ptprz1*-C1 (ACD Biotechne, 460991).

For lineage tracing experiments and the identification of P60 OL lineage with tissue from the Pdgfrα::$CreER^{T1}$-RCE::LoxP-GFP mice (*20, 51*), the RNAscope ISH was coupled with IHC to detect the GFP reporter or endogenous Sox10. Briefly, after hybridization and amplification steps to detect the mRNA of the target gene markers, the sections were blocked in 5% normal donkey serum (NDS), 0.03% Triton X100 in PBS for 1h at RT and incubated with chicken anti-GFP (AbCam, ab 13970) or goat anti-Sox10 (Santa Cruz, sc-17342) primary antibodies 1:200 in 2% NDS, 0.03% Triton X100 in PBS, O.N. at RT. The following day, the sections were incubated with goat anti-chicken AlexaFluor 488 conjugated (AbCam, ab150169) or donkey anti-goat AlexaFluor 647 conjugated (LifeTech, A21447) secondary antibodies 1:500 in 2% NDS, 0.03% Triton X100 in PBS, 1h at RT and counterstained with DAPI (1:5,000 in PBS) for 2 min. IHC washing steps were performed with 0.05% Tween-20 in PBS.

Image acquisition

Fluorescent images were acquired using the LSM800 confocal microscope set up (Zeiss). To obtain an optimal balance between resolution of RNAscope signal and imaged area, tiled images were acquired with a 40X water objective. The z-stack was kept to 2-3 focal planes with 40 µm step to reduce the probability of false positive cells after image maximum projection.

Image analysis

Confocal images were processed with FiJi (ImageJ, NIH) to select the regions of interest (ROIs). ROI images were segmented with a customized CellProfiler pipeline. Briefly, the signals from the individual channels (DAPI, markers, GFP) were segmented; OL lineage cells ($Sox10^+$) were identified using the masking option with the DAPI counterstain. Then, the specific OL lineage populations were identified using the relate objects options with the $Sox10^+$ or $Sox10^+$-GFP^+ cells. Overlay images of the identified objects were exported and used to assess the percentage of cell segmentation error. Spreadsheets containing the number of parent cells (DAPI, $Sox10^+$ or $Sox10^+$-GFP^+ cells) and child objects (*Ptgds*$^+$, *Klk6*$^+$, *Egr2*$^+$, *Ptprz1*$^+$) were exported and used to calculate the percentage of each population. Based on the average gene expression in scRNAseq dataset (*2*), we used a cut off of 12, 4, 3, and 7 molecules of *Ptgds*$^+$, *Klk6*$^+$, *Egr2*$^+$, *Ptprz1*$^+$, respectively, per cells to call the analyzed OL lineage populations.

We manually assessed the percentage of error for the automated cell segmentation and attribution on 18 representative images (six images per analyzed region). We recorded a segmentation error in the identification of the nuclei of 6.40 ± 1.07% (SFig.1D). We did not observe any substantial error additional to the nuclei segmentation error when we identified the $Sox10^+$-GFP^+ nuclei by the masking option (SFig.1D). Our analysis is a reliable tool for the fast quantification of cells in large image datasets. We calculated the percentage of cells belonging to the oligodendrocyte lineage over the total number of cells ($DAPI^+$ nuclei) and detected the highest and lowest percentage in the corpus callosum and cortex at both P20 (65.87 ± 2.26% and 10.3 ± 0.62%) and P60 (67.95 ± 4.78% and 20.0 ± 5.13%), respectively (SFig.1B). This is in line with the previously described distribution of the OL lineage (*58*) and the relatively myelination levels of the analyzed regions.

Clustering analysis

Cells were analyzed using the scater package (10.1093/bioinformatics/btw777). Cells with less than 100 UMI counts and more than 15,000 were not considered for downstream analysis. Pool normalization was then used for normalization the expression matrix (https://doi.org/10.1186/s13059-016-0947-7), feature selection was performed by calculating the

coefficient of variation and using support vector regression to predict variance for a given gene expression level, all genes showing higher variance than expected were used for downstream analysis. The GeneFocus pipeline(*18*) was used for gene filtering and Spearman correlation was used to build a KNN-graph after which Louvain clustering was applied. Cells that did not include any shared nearest neighbors were discarded from the clustering as outliers. Due to the limited number of cells present in some populations, we performed additional hierarchical clustering and set the threshold to separate the three main populations, oligodendrocyte progenitor cells (OPCs), committed oligodendrocyte progenitor cells (COPs), and mature oligodendrocytes (MOLs). The hierarchical and Louvain clusters were then combined, where the addition of the hierarchical clustering results led to the separation of COP cluster from the broader original Louvain clusters containing both OPCs and COPs.

Categorization of OL clusters in MOL1, MOL2, or MOL5/6 clusters corresponds to the cluster wide expression of Egr2 for MOL1, Sepp1/Hopx/Klk6 for MOL2, and Opalin/Ptgds for MOL5/6.

Statistics

Statistics on the spatial distribution of the OL lineage populations was performed using 2-way ANOVA. For multiple comparison analysis, the Sidak's correction was applied.

Differential gene expression analysis was performed using pairwise Wilcoxon rank sum tests using the stats package in R, on averaged expression per cluster. Significant genes were selected with a FDR adjusted p-value <0.01. The heatmap displays the most top 20 highest enriched genes as measured by z-score.

Code availability

Code used for scRNAseq analysis is available at https://github.com/Castelo-Branco-lab/GeneFocus.

Figure legends

Fig. 1. Specific mature OL populations have spatial preference in the juvenile and adult central nervous system. (**A-B**) Schematics of coronal sections of the mouse brain (A) and spinal cord (B). Red squares highlight the systematically analyzed CNS regions. (**C-F**) Confocal representative images of the distribution of OPC-COPs (*Ptprz1*$^+$ OL lineage cells. C), MOL5/6 (*Ptgds*$^+$ OL lineage cells. D), MOL2 (*Klk6*$^+$ OL lineage cells. E), and MOL1 (*Egr2*$^+$ OL lineage cells. F) in the dorsal horn (grey matter) of the juvenile (P20) and adult (P60) spinal cord. Scale bar

= 20 µm. (**G-J**) Quantification of the OPCs-COPs (G), MOL5/6 (H), MOL2 (I), and MOL1 (J) distribution in the cortex, corpus callosum, and dorsal horn in juvenile (P20) and adulthood (P60). Percentage of the population is calculated on the total number of OL lineage cells (*Sox10*$^+$ cells) in the analyzed region. Data are presented as Mean ± SEM. n = 6-9 per condition. Asterisks indicate a significant difference between conditions (*p ≤ 0.05, **p ≤ 0.01, ***p ≤ 0.001, ****p ≤ 0.0001, 2-way ANOVA with Sidak's correction). Cx = cortex, CC = corpus callosum, SC = spinal cord.

Fig. 2. MOL2 and MOL5/6 are specifically enriched in adjacent regions of the juvenile and adult spinal cord. (**A**) Schematics of a coronal section of the spinal cord. Highlighted in blue and red the white matter regions where the axons forming the dorsal columns and dorsal corticospinal tract run, respectively. (**B, D**) Confocal representative images show the enrichment of MOL2 (*Klk6*$^+$ OL lineage cells) in the white matter of the spinal cord (B) and at the level of the dorsal columns (D). (**F, H**) Confocal representative images show the enrichment of MOL5/6 (*Ptgds*$^+$ OL lineage cells) in the grey matter of the spinal cord (F) and at the level of the dorsal corticospinal tract (H). Scale bar = 100. (**C, E, G, I**) Quantification of the MOL2 and MOL5/6 distribution in the white and grey matter of the spinal cord (C, G) and at the level of the dorsal corticospinal tract and dorsal columns (E, I) in juvenile (P20) and adulthood (P60). Percentage of the population is calculated on the total number of OL lineage cells (*Sox10*$^+$ cells) in the analyzed region. Data are presented as Mean ± SEM. n = 3-9 per condition. Asterisks indicate a significant difference between conditions (*p ≤ 0.05, **p ≤ 0.01, ***p ≤ 0.001, 2-way ANOVA with Sidak's correction). GM = grey matter, WM = white matter, DC = dorsal columns, dCST = dorsal corticospinal tract.

Fig. 3. The developmental origin of MOLs is not relevant for their identity in adulthood. (**A**) Confocal representative images of the P90 brain from Emx1::Cre-SOX10::GFP-TdTom mouse. Dashed outline highlights the corpus callosum and dissected region used for scRNAseq. (**B-C**) t-Distributed stochastic neighbor embedding (t-SNE) plots showing the OL lineage composition categorized by expression of markers characterizing the major OL populations (B) and the TdTom$^+$ and GFP$^+$ OL lineage cells contribution to the clusters. (**D**) Frequency distribution of the TdTom$^+$ and GFP$^+$ OL lineage cells forming the major clusters. (**E**) Schematic overview of the fate mapping experimental design. Green arrows shows the GFP expression timeline 24h delayed from the time of tamoxifen injection. (**F**) Confocal representative images show the MOL2 (*Klk6*$^+$-GFP$^+$ OL lineage cells) and MOL5/6 (*Ptgds*$^+$-GFP$^+$ OL lineage cells. G) differentiated from pre- (TM E12.5) or postnatal (TM P3-5) OPCs. Scale bar = 20 µm. (**G**) Percentages of the fate mapped OPCs-COPs (*Ptprz1*$^+$-GFP$^+$ OL lineage cells), MOL1 (*Egr2*$^+$-GFP$^+$ OL lineage cells), MOL2 (*Klk6*$^+$-GFP$^+$ OL lineage cells), and MOL5/6 (*Ptgds*$^+$-GFP$^+$ OL lineage cells) populations are calculated on the total

number of fate mapped OL lineage cells (*Sox10*$^+$-GFP$^+$ cells) in the juvenile and adult corpus callosum. Data are presented as Mean ± SEM. n = 3-5 per condition. Asterisks indicate a significant difference between conditions (**p ≤ 0.01, ***p ≤ 0.0001, 2-way ANOVA with Sidak's correction). TM = tamoxifen.

Fig. 4. MOL2 and MOL5/6 show differential susceptibility to spinal cord injury. (**A-C**) Schematic of the analysis lesion model (A), timeline (B), injury level (T10) and distance of the rostral and caudal analyzed segments (C). (**D-E**) Confocal representative images of the rostral (D) and injury sites (E) showing the specific loss of MOL2 and the high repopulation by MOL5/6 of the injury site as well as the maintained MOL2 (*Klk6*$^+$ OL lineage cells) and MOL5/6 (*Ptgds*$^+$ OL lineage cells) adjacent spatial preference away (10-5 mm) from the injury site. White and yellow dashed lines highlight the dorsal funiculi and lesion site, respectively. White rectangles highlight the regions shown in higher magnification. Scale bar = 100 µm. (**F-G**) Percentages of the populations are calculated on the total number of OL lineage cells (*Sox10*$^+$ cells) in the analyzed segments 3 (F) and 5 (G) mpi. Data are presented as Mean ± SEM. n = 3-7 per condition. Asterisks indicate a significant difference between conditions (*p ≤ 0.05, **p ≤ 0.01, 2-way ANOVA with Sidak's correction). SCI = spinal cord injury, mpi = months post-injury, DC = dorsal columns, dCST = dorsal corticospinal tract, GM = grey matter, WM = white matter, T10 = thoracic vertebra 10.

Fig. S1. Automated image analysis pipeline and validation. (**A**) Schematic overview and representative analyzed image output of the customized CellProfiler pipeline used in this study. (**B-C**) Percentage of the OL lineage cells (*Sox10*$^+$ cells) calculated on the total number of nuclei shows the expected differential enrichment of the OL lineage in the analyzed regions. (**D**) Percentage of the segmentation error of the used pipeline. Data are presented as Mean ± SEM. n = 5-18 per condition. Asterisks indicate a significant difference between conditions (**p ≤ 0.01, 2-way ANOVA with Sidak's correction). Cx = cortex, CC = corpus callosum, SC = spinal cord, DC = dorsal columns, dCST = dorsal corticospinal tract.

Fig. S2. Differential distribution of specific OL lineage populations/states in the juvenile and adult central nervous system. (**A-H**)Confocal representative images of the distribution of OPC-COPs (*Ptprz1*$^+$ OL lineage cells. A, E), MOL5/6 (*Ptgds*$^+$ OL lineage cells. B, F), MOL2 (*Klk6*$^+$ OL lineage cells. C, G), and MOL1 (*Egr2*$^+$ OL lineage cells. D, H) in the juvenile (P20) and adult (P60) cortex (A-D) and corpus callosum (E-H). Scale bar = 20 µm.

Fig. S3. Louvain clustering analysis of the OL lineage cells. (**A**) t-Distributed stochastic neighbor embedding (t-SNE) plots showing the OL lineage composition determined by hierarchical clustering. (**B**) Frequency distribution of the TdTom+ and GFP+ OL lineage cells forming each identified cluster. (**C**) Heat-map of differential gene expression highlighting the enriched gene modules (right) characterizing the identified clusters (above and below) by Louvain clustering analysis. Distance matrix = Spearmann correlation.

Fig. S4. Pre- and postnatal-OPCs can equally contribute to the generation of MOL populations in the adult central nervous system. (**A-D, F-L**) Confocal representative images show embryonically (TM E12.5)- and postnatally (TM P3-5)-derived OPCs-COPs (*Ptprz1*$^+$-GFP$^+$ OL lineage cells. A, F, I), MOL5/6 (*Ptgds*$^+$-GFP$^+$ OL lineage cells. B, J), MOL2 (*Klk6*$^+$-GFP$^+$ OL lineage cells. C, G, K), MOL1 (*Egr2*$^+$-GFP$^+$ OL lineage cells. D, H, L) in the adult (P60) cortex (A-D), corpus callosum (F-H), and dorsal horn of the spinal cord (I-L). Scale bar = 20 μm. (**E-L**) Percentages of the fate mapped OPCs-COPs (*Ptprz1*$^+$-GFP$^+$ OL lineage cells), MOL1 (*Egr2*$^+$-GFP$^+$ OL lineage cells), MOL2 (*Klk6*$^+$-GFP$^+$ OL lineage cells), and MOL5/6 (*Ptgds*$^+$-GFP$^+$ OL lineage cells) populations are calculated on the total number of fate mapped OL lineage cells (*Sox10*$^+$ -GFP$^+$ cells) in the juvenile and adult cortex (E) and spinal cord (M). (**N**) Percentages of the embryonically (TM E12.5)- and postnatally (TM P3-5)-derived MOL2 (*Klk6*$^+$-GFP$^+$ OL lineage cells), and MOL5/6 (*Ptgds*$^+$-GFP$^+$ OL lineage cells) populations are calculated on the total number of fate mapped OL lineage cells (*Sox10*$^+$ -GFP$^+$ cells) in the spinal cord white and grey matter. Data are presented as Mean ± SEM. n = 3-5 per condition. Asterisks indicate a significant difference between conditions (*p ≤ 0.05, **p ≤ 0.01, ***p ≤ 0.001, ***p ≤ 0.0001, 2-way ANOVA with Sidak's correction). TM = tamoxifen.

Fig. S5. MOL2 population expands away form the injury site but maintain its spatial preference following spinal cord injury. (**A**) Confocal representative images of the rostral, caudal, and injury sites showing the specific loss of MOL2 and the high repopulation by MOL5/6 of the injury site as well as the maintained MOL2 (*Klk6*$^+$ OL lineage cells) and MOL5/6 (*Ptgds*$^+$ OL lineage cells) adjacent spatial preference away (10-5 mm) from the injury site, 3 months post-injury. White and yellow dashed lines highlight the dorsal funiculi and lesion site, respectively. Scale bar = 100 μm. (**B-C, F-I**) Percentages of the MOL2 (*Klk6*$^+$ OL lineage cells. B, F-I) and MOL5/6 (*Ptgds*$^+$ OL lineage cells. C, F-I) populations are calculated on the total number of OL lineage cells (*Sox10*$^+$ cells) in the dorsal funiculi region (B-C) and their differential distribution at the level of the dorsal columns (F, H) and dorsal corticospinal tract (G, I) 5-10mm rostral and caudal to the injury site. (**D-E**) Percentages of the OL lineage cells (*Sox10*$^+$ cells) are calculated on the total number of nuclei in

the analyzed segments 3 (D) and 5 (E) mpi. Dashed grey line marks the average percentage of the OL lineage cells in the intact adult spinal cord. Data are presented as Mean ± SEM. n = 3-7 per condition. Asterisks indicate a significant difference between conditions (*p ≤ 0.05, **p ≤ 0.01, ***p≤ 0.001, 2-way ANOVA with Sidak's correction). mpi = months post-injury.

Table 1. Counting of analyzed cells by scRNAseq.

References

1. M. Simons, K. A. Nave, Oligodendrocytes: Myelination and Axonal Support. *Cold Spring Harbor perspectives in biology* **8**, a020479 (2015).
2. S. Marques *et al.*, Oligodendrocyte heterogeneity in the mouse juvenile and adult central nervous system. *Science* **352**, 1326-1329 (2016).
3. S. Marques *et al.*, Transcriptional Convergence of Oligodendrocyte Lineage Progenitors during Development. *Dev Cell* **46**, 504-517 e507 (2018).
4. A. M. Falcão *et al.*, Disease-specific oligodendrocyte lineage cells arise in multiple sclerosis. *Nature Medicine*, (2018).
5. A. H. Crawford, R. B. Tripathi, W. D. Richardson, R. J. Franklin, Developmental Origin of Oligodendrocyte Lineage Cells Determines Response to Demyelination and Susceptibility to Age-Associated Functional Decline. *Cell Rep*, (2016).
6. G. S. Tomassy *et al.*, Distinct profiles of myelin distribution along single axons of pyramidal neurons in the neocortex. *Science* **344**, 319-324 (2014).
7. K. D. Micheva *et al.*, A large fraction of neocortical myelin ensheathes axons of local inhibitory neurons. *Elife* **5**, (2016).
8. G. S. Tomassy, L. B. Dershowitz, P. Arlotta, Diversity Matters: A Revised Guide to Myelination. *Trends Cell Biol* **26**, 135-147 (2016).
9. M. E. Bechler, L. Byrne, C. Ffrench-Constant, CNS Myelin Sheath Lengths Are an Intrinsic Property of Oligodendrocytes. *Curr Biol* **25**, 2411-2416 (2015).
10. E. G. Baxi *et al.*, Lineage tracing reveals dynamic changes in oligodendrocyte precursor cells following cuprizone-induced demyelination. *Glia* **65**, 2087-2098 (2017).
11. S. Liu, C. Trapnell, Single-cell transcriptome sequencing: recent advances and remaining challenges. *F1000Res* **5**, (2016).
12. S. C. van den Brink *et al.*, Single-cell sequencing reveals dissociation-induced gene expression in tissue subpopulations. *Nat Methods* **14**, 935-936 (2017).
13. L. Cantuti-Castelvetri *et al.*, Defective cholesterol clearance limits remyelination in the aged central nervous system. *Science*, (2018).
14. F. J. Sim, C. Zhao, J. Penderis, R. J. Franklin, The age-related decrease in CNS remyelination efficiency is attributable to an impairment of both oligodendrocyte progenitor recruitment and differentiation. *J Neurosci* **22**, 2451-2459 (2002).
15. S. A. Shields, J. M. Gilson, W. F. Blakemore, R. J. Franklin, Remyelination occurs as extensively but more slowly in old rats compared to young rats following gliotoxin-induced CNS demyelination. *Glia* **28**, 77-83 (1999).
16. M. S. Yeung *et al.*, Dynamics of oligodendrocyte generation and myelination in the human brain. *Cell* **159**, 766-774 (2014).
17. R. B. Tripathi *et al.*, Dorsally and ventrally derived oligodendrocytes have similar electrical properties but myelinate preferred tracts. *J Neurosci* **31**, 6809-6819 (2011).
18. A. M. Falcao *et al.*, Disease-specific oligodendrocyte lineage cells arise in multiple sclerosis. *Nat Med* **24**, 1837-1844 (2018).
19. A. Zeisel *et al.*, Brain structure. Cell types in the mouse cortex and hippocampus revealed by single-cell RNA-seq. *Science* **347**, 1138-1142 (2015).
20. S. H. Kang, M. Fukaya, J. K. Yang, J. D. Rothstein, D. E. Bergles, NG2+ CNS glial progenitors remain committed to the oligodendrocyte lineage in postnatal life and following neurodegeneration. *Neuron* **68**, 668-681 (2010).
21. C. S. Ahuja *et al.*, Traumatic spinal cord injury. *Nat Rev Dis Primers* **3**, 17018 (2017).
22. E. Emery *et al.*, Apoptosis after traumatic human spinal cord injury. *J Neurosurg* **89**, 911-920 (1998).
23. A. Almad, F. R. Sahinkaya, D. M. McTigue, Oligodendrocyte fate after spinal cord injury. *Neurotherapeutics* **8**, 262-273 (2011).

24. S. Casha, W. R. Yu, M. G. Fehlings, Oligodendroglial apoptosis occurs along degenerating axons and is associated with FAS and p75 expression following spinal cord injury in the rat. *Neuroscience* **103**, 203-218 (2001).
25. G. L. Li, M. Farooque, A. Holtz, Y. Olsson, Apoptosis of oligodendrocytes occurs for long distances away from the primary injury after compression trauma to rat spinal cord. *Acta Neuropathol* **98**, 473-480 (1999).
26. J. M. Lytle, J. R. Wrathall, Glial cell loss, proliferation and replacement in the contused murine spinal cord. *Eur J Neurosci* **25**, 1711-1724 (2007).
27. P. Warden *et al.*, Delayed glial cell death following wallerian degeneration in white matter tracts after spinal cord dorsal column cordotomy in adult rats. *Exp Neurol* **168**, 213-224 (2001).
28. D. Purger, E. M. Gibson, M. Monje, Myelin plasticity in the central nervous system. *Neuropharmacology* **110**, 563-573 (2016).
29. L. Filli, M. E. Schwab, Structural and functional reorganization of propriospinal connections promotes functional recovery after spinal cord injury. *Neural Regen Res* **10**, 509-513 (2015).
30. K. Minassian, W. B. McKay, H. Binder, U. S. Hofstoetter, Targeting Lumbar Spinal Neural Circuitry by Epidural Stimulation to Restore Motor Function After Spinal Cord Injury. *Neurotherapeutics* **13**, 284-294 (2016).
31. J. R. Leslie *et al.*, Ectopic myelinating oligodendrocytes in the dorsal spinal cord as a consequence of altered semaphorin 6D signaling inhibit synapse formation. *Development* **138**, 4085-4095 (2011).
32. J. P. Kapfhammer, M. E. Schwab, Inverse patterns of myelination and GAP-43 expression in the adult CNS: neurite growth inhibitors as regulators of neuronal plasticity? *J Comp Neurol* **340**, 194-206 (1994).
33. J. H. Martin, The corticospinal system: from development to motor control. *Neuroscientist* **11**, 161-173 (2005).
34. E. A. Joosten, A. A. Gribnau, P. J. Dederen, Postnatal development of the corticospinal tract in the rat. An ultrastructural anterograde HRP study. *Anat Embryol (Berl)* **179**, 449-456 (1989).
35. M. W. Fox, O. R. Inman, W. A. Himwich, The postnatal development of the spinal cord of the dog. *J Comp Neurol* **130**, 233-240 (1967).
36. R. B. Tripathi *et al.*, Remarkable Stability of Myelinating Oligodendrocytes in Mice. *Cell Rep* **21**, 316-323 (2017).
37. J. R. Wolpaw, Spinal cord plasticity in acquisition and maintenance of motor skills. *Acta Physiol (Oxf)* **189**, 155-169 (2007).
38. I. A. McKenzie *et al.*, Motor skill learning requires active central myelination. *Science* **346**, 318-322 (2014).
39. W. Olson, P. Dong, M. Fleming, W. Luo, The specification and wiring of mammalian cutaneous low-threshold mechanoreceptors. *Wiley Interdiscip Rev Dev Biol* **5**, 389-404 (2016).
40. W. Luo, H. Enomoto, F. L. Rice, J. Milbrandt, D. D. Ginty, Molecular identification of rapidly adapting mechanoreceptors and their developmental dependence on ret signaling. *Neuron* **64**, 841-856 (2009).
41. B. A. Barres *et al.*, Cell death and control of cell survival in the oligodendrocyte lineage. *Cell* **70**, 31-46 (1992).
42. L. O. Sun *et al.*, Spatiotemporal Control of CNS Myelination by Oligodendrocyte Programmed Cell Death through the TFEB-PUMA Axis. *Cell* **175**, 1811-1826 e1821 (2018).
43. W. D. Richardson, N. Kessaris, N. Pringle, Oligodendrocyte wars. *Nat Rev Neurosci* **7**, 11-18 (2006).
44. M. Fogarty, W. D. Richardson, N. Kessaris, A subset of oligodendrocytes generated from radial glia in the dorsal spinal cord. *Development* **132**, 1951-1959 (2005).
45. N. Kessaris *et al.*, Competing waves of oligodendrocytes in the forebrain and postnatal elimination of an embryonic lineage. *Nat Neurosci* **9**, 173-179 (2006).
46. O. Marin, J. L. Rubenstein, A long, remarkable journey: tangential migration in the telencephalon. *Nat Rev Neurosci* **2**, 780-790 (2001).
47. J. Briscoe, A. Pierani, T. M. Jessell, J. Ericson, A homeodomain protein code specifies progenitor cell identity and neuronal fate in the ventral neural tube. *Cell* **101**, 435-445 (2000).
48. C. Schuurmans, F. Guillemot, Molecular mechanisms underlying cell fate specification in the developing telencephalon. *Current opinion in neurobiology* **12**, 26-34 (2002).
49. B. E. Powers *et al.*, Remyelination reporter reveals prolonged refinement of spontaneously regenerated myelin. *Proc Natl Acad Sci U S A* **110**, 4075-4080 (2013).
50. S. Jakel *et al.*, Altered human oligodendrocyte heterogeneity in multiple sclerosis. *Nature* **566**, 543-547 (2019).
51. S. J. Butt *et al.*, The requirement of Nkx2-1 in the temporal specification of cortical interneuron subtypes. *Neuron* **59**, 722-732 (2008).
52. C. Laranjeira *et al.*, Glial cells in the mouse enteric nervous system can undergo neurogenesis in response to injury. *J Clin Invest* **121**, 3412-3424 (2011).
53. X. Mao, Y. Fujiwara, A. Chapdelaine, H. Yang, S. H. Orkin, Activation of EGFP expression by Cre-mediated excision in a new ROSA26 reporter mouse strain. *Blood* **97**, 324-326 (2001).
54. S. Hayashi, P. Lewis, L. Pevny, A. P. McMahon, Efficient gene modulation in mouse epiblast using a Sox2Cre transgenic mouse strain. *Mech Dev* **119 Suppl 1**, S97-S101 (2002).
55. E. Nakamura, M. T. Nguyen, S. Mackem, Kinetics of tamoxifen-regulated Cre activity in mice using a cartilage-specific CreER(T) to assay temporal activity windows along the proximodistal limb skeleton. *Dev Dyn* **235**, 2603-2612 (2006).

56. M. Valny, P. Honsa, D. Kirdajova, Z. Kamenik, M. Anderova, Tamoxifen in the Mouse Brain: Implications for Fate-Mapping Studies Using the Tamoxifen-Inducible Cre-loxP System. *Front Cell Neurosci* **10**, 243 (2016).
57. N. Wilking, L. E. Appelgren, K. Carlstrom, A. Pousette, N. O. Theve, The distribution and metabolism of 14C-labelled tamoxifen in spayed female mice. *Acta Pharmacol Toxicol (Copenh)* **50**, 161-168 (1982).
58. C. S. von Bartheld, J. Bahney, S. Herculano-Houzel, The search for true numbers of neurons and glial cells in the human brain: A review of 150 years of cell counting. *Journal of Comparative Neurology* **524**, 3865-3895 (2016).

Floriddia et al, Fig. 1

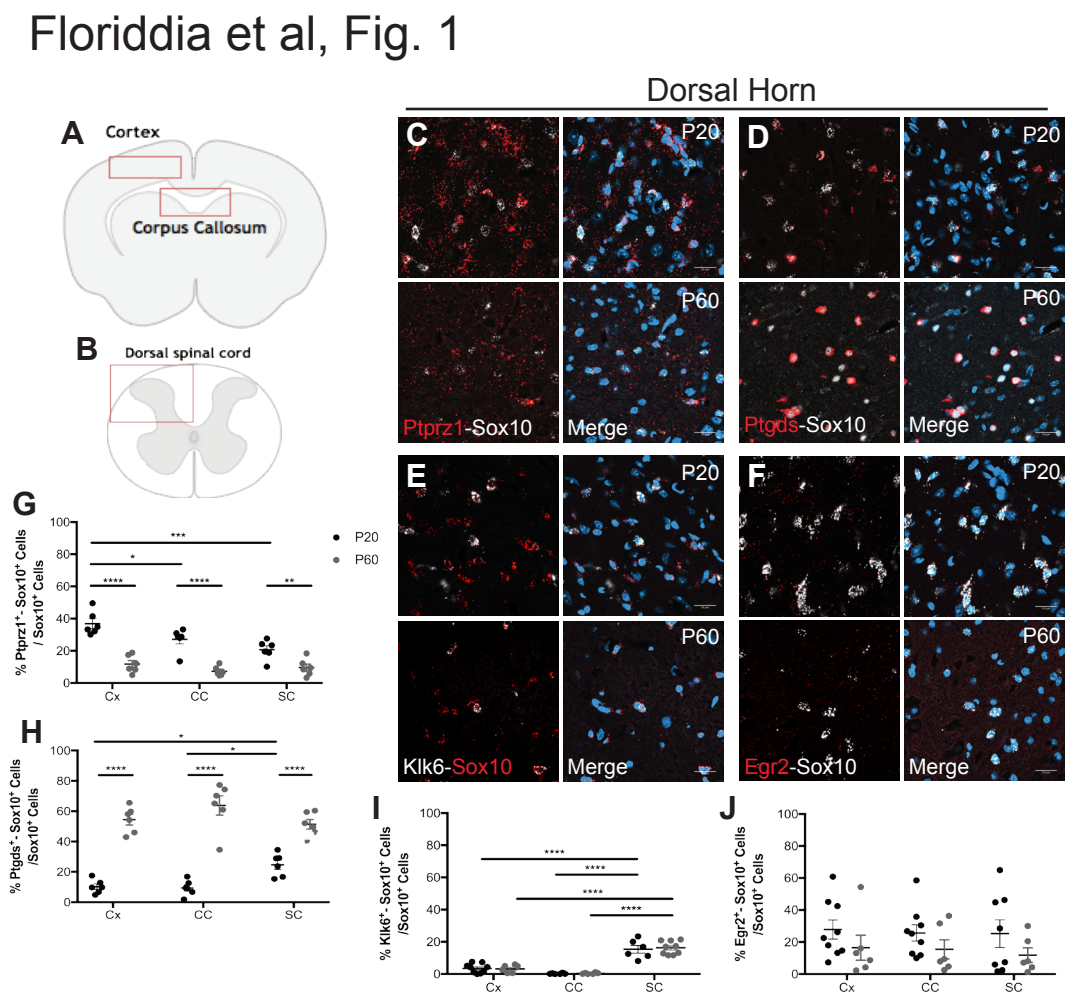

Floriddia et al, Fig. 2

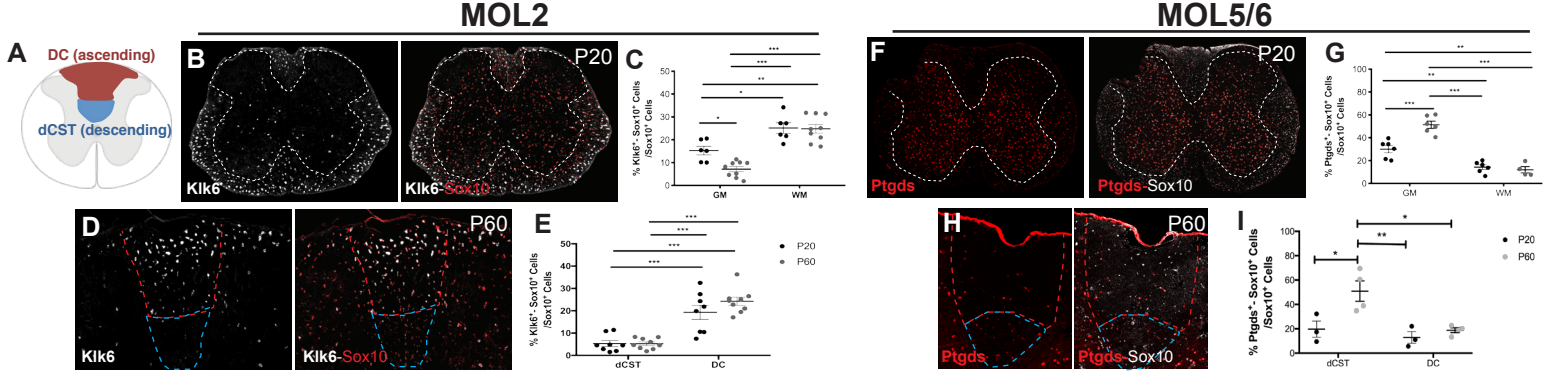

Floriddia et al, Fig. 3

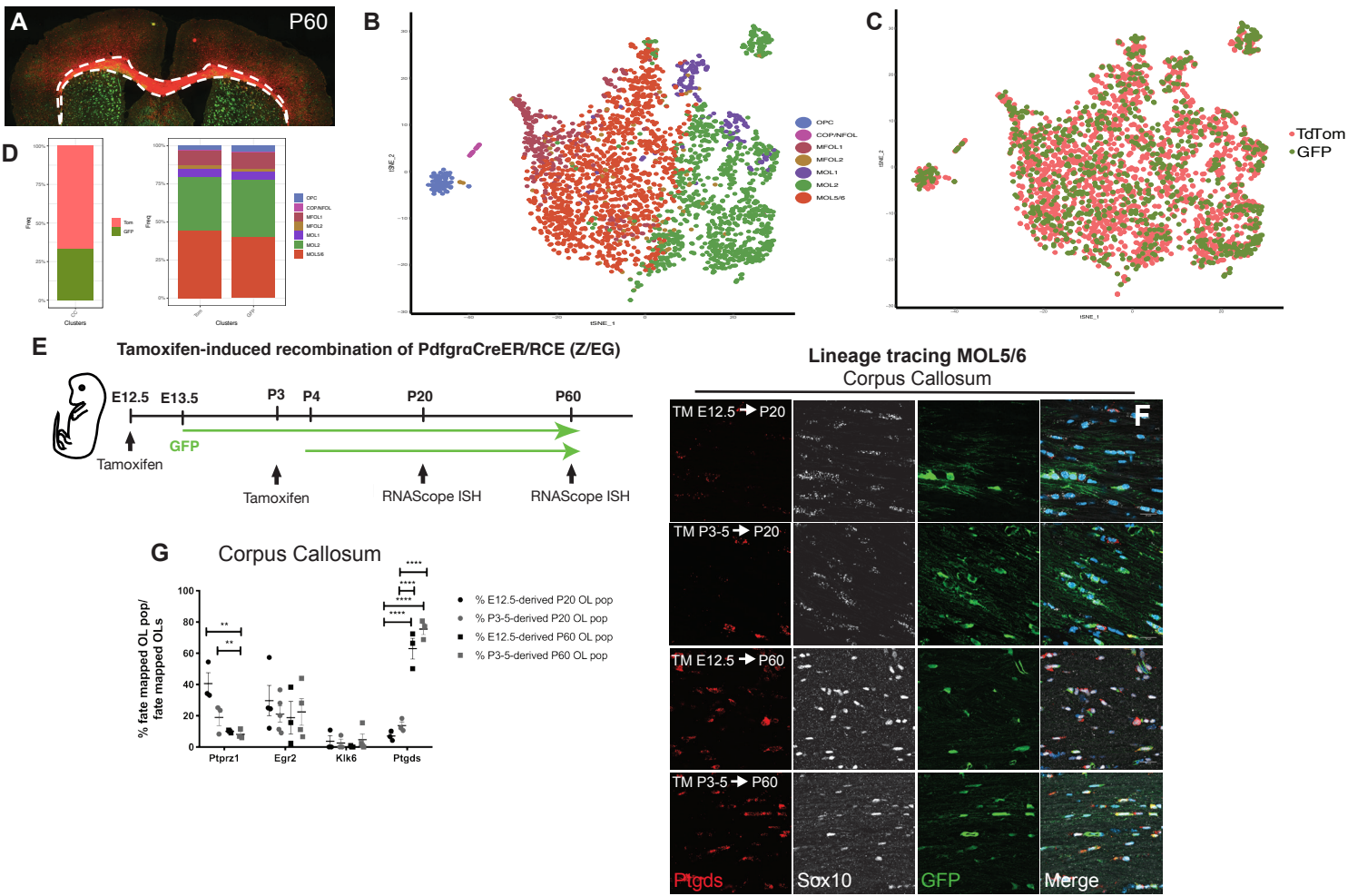

Floriddia et al., Fig. 4